



TECHNICAL ARTICLE

Interfacial Microstructure and Mechanical Properties of Explosively Welded Mg/Al Alloy Plates

Mami Mihara-Narita, Konosuke Asai, Hisashi Sato, Yoshimi Watanabe, Hisashi Mori, Naobumi Saito, and Yasumasa Chino

Submitted: 30 November 2021 / Revised: 23 February 2022 / Accepted: 20 March 2022 / Published online: 12 April 2022

The interfacial microstructure and hardness of cladding plates produced by explosive welding between magnesium alloys having different aluminum concentrations and A6005C aluminum alloy were investigated. Further, measurements of residual stress at the interface of cladding plates were performed. In all cladding plates, the bonding interface had a wavy shape. Adiabatic shear bands were formed at the interface on the magnesium alloy side and deformation twins appeared at the interface due to the impact of explosive welding. Microstructure observation using scanning transmission electron microscope revealed that a thin interlayer was formed at the interface in all cladding plates. The thickness of the interlayer increased with an increase in aluminum concentration in the magnesium alloy, while the thickness was 1 μm or less. In the cross-section of the cladding plate, aluminum alloy showed a relatively higher Vickers hardness value compared with the magnesium alloy, and the hardness value increased when approaching the interface. However, nanoindentation tests revealed no increase in hardness was observed at the interface. Measurements of the residual stress using synchrotron radiation x-rays at the interface of cladding plates revealed a tendency for the occurrence of tensile residual stress on the magnesium alloy side and compressive residual stress on the aluminum alloy side. This might be due to a difference in the coefficient of thermal expansion between the magnesium and aluminum alloys.

Keywords aluminum, dissimilar metal joining, explosive welding, interlayer, magnesium, residual stress

1. Introduction

In terms of environmental protection, using a lightweight vehicle body leads to less CO₂ emissions. The aluminum alloys, magnesium alloys, carbon fiber composite materials, etc., which are developed to achieve weight reduction, are good candidates for new lightweight materials. Therefore, “multi-materialization,” produced by joining dissimilar materials, has received intense interest.

Magnesium alloys are the lightest of all practical alloys and have a large weight-reducing effect, so they are expected to be applied to vehicle bodies. While efforts are being made on

many subjects, such as the rolling costs of magnesium alloys and their molding process, the development of a composite material (cladding plate between magnesium alloys and aluminum alloys) is drawing attention. If the cladding plate can be used as a vehicle body, a weight reduction can be expected.

Regarding the joining of magnesium alloys and aluminum alloys, various methods such as melt welding (Ref 1), diffusion welding (Ref 2), hot press (Ref 3), friction stir welding (FSW) (Ref 4, 5) have been studied. But the mechanical properties of the bonding material decrease due to the formation of brittle Al-Mg-based intermetallic compounds. Figure 1 shows the equilibrium phase diagram of the Al-Mg system (Ref 6). Magnesium and Aluminum have similar melting points and can form stable intermediate phases such as $\beta\text{-Mg}_2\text{Al}_3$ or $\gamma\text{-Mg}_{17}\text{Al}_{12}$ in their equilibrium phase. In diffusion bonding and FSW, which are solid-phase bonding the relatively high bonding strength can be obtained, but the above-mentioned intermetallic compounds are also formed by these bonding methods, which affects the mechanical properties and the bonding process time. Due to the increased bonding process time and high cost, the development of new joining methods is required.

In this research, the “explosive welding method” (Ref 7, 8), which is a type of solid-phase welding, is investigated. The explosive welding method is a method that utilizes the instantaneous high energy generated by the explosion of explosives for metal bonding and has almost no thermal effect except for local heat generation near the bonding interface (Ref 8). During the explosive welding, high-speed metal jets are generated between the base and flyer plate; this removes the

This article is an invited submission to the *Journal of Materials Engineering and Performance* selected from presentations at the symposium “Joining,” belonging to the area “Processing” at the European Congress and Exhibition on Advanced Materials and Processes (EUROMAT 2021), held virtually from September 12–16, 2021, and has been expanded from the original presentation.

Mami Mihara-Narita, Konosuke Asai, Hisashi Sato, and Yoshimi Watanabe, Department of Physical Science and Engineering, Nagoya Institute of Technology, Showa-ku, Gokisocho, Nagoya 466-8555, Japan; **Hisashi Mori**, Research & Development Division, UACJ Corporation, Nagoya, Japan; and **Naobumi Saito and Yasumasa Chino**, National Institute of Advanced Industrial Science and Technology (AIST), Nagoya, Japan. Contact e-mail: narita.mami@nitech.ac.jp.

surface oxide film and the fresh surfaces are bonded together (Ref 9). There is no time for a heat transfer and large-scale melting to take place during welding, thus the number of intermetallic compounds formed during explosive welding is less than other welding method, such as melt welding. In addition, direct joining of dissimilar metals that are difficult to be welded by other welding method can be achieved using explosive welding (Ref 10). This method has already been applied in the fields of steel and aluminum alloys and is used for structural members for ships (Ref 11). Further, explosive welding of metal foils (EWMF), which joints metal foils and base metal plate through high-speed oblique impact, has received much attentions (Ref 12-14). Similar to the explosive welding of dissimilar metals, wavy interface and local molten zone which is also called vortices or eddies at the crest is obtained during EWMF (Ref 12). These zones representatively show complex microstructures such as formation of amorphous (Ref 15), nanoscale grains (Ref 16), intermetallics (Ref 17, 18), and recrystallized grains (Ref 19), which affect the bonding strength of the joint. Regarding the joining of magnesium alloys and aluminum alloys using the explosive welding method, the microstructure of the interface and mechanical properties of the explosively welded material have been reported only for specific alloy compositions (Ref 20, 21). Recently, the effects of the aluminum concentration in the magnesium alloy on interfacial microstructure, corrosion resistance and mechanical properties are studied for the first time (Ref 22), however, the detailed hardness, nanomechanical properties, and residual stress near the interface which are

necessary for practical use are still lacking. The aim of this study is to evaluate the effect of the composition of magnesium alloy on the evolution of interfacial microstructure, hardness, and nanomechanical properties of explosively welded magnesium alloy/aluminum alloy cladding plates. Furthermore, residual stress states at the interface were also investigated. It is thought that the grain refinement, dislocation density increment, formation of deformation twins, etc. affect macro mechanical properties of explosive welded cladding plates. However, at the interface, they are in a nonuniform state. In this study, characterization of the entire cladding plate and the interface from the perspective of hardness and residual stress is conducted.

Explosive welding generates residual stress in the composite plate (Ref 23). The residual stress originates as a result of severe plastic deformation, local melted material during

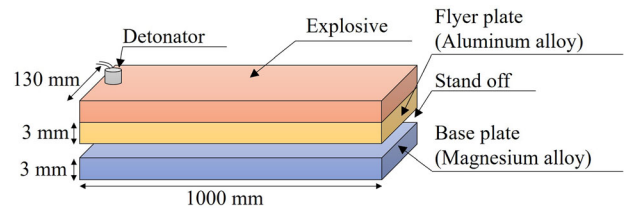


Fig. 2 Experimental setup for the explosive welding process

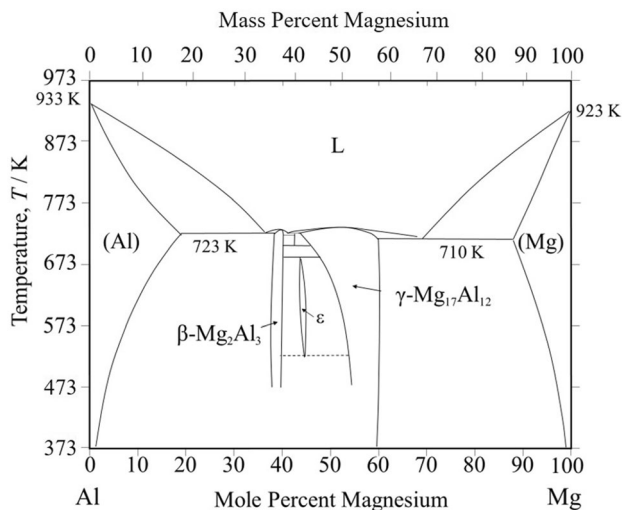


Fig. 1 Al-Mg binary phase diagram

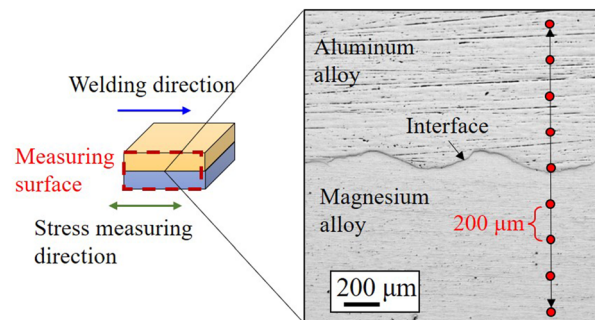


Fig. 3 Schematic illustration for the specimen and measurement points of residual stress measurement

Table 2 The wavy length and the amplitude of each samples interface

Sample	Wavelength (mm)	Amplitude (mm)
AZ31/A6005C	0.77	0.14
AZ61/A6005C	0.76	0.13
AZ80/A6005C	0.65	0.11

Table 1 Chemical compositions of the investigated alloys (mass %)

	Mg	Al	Zn	Si	Mn	Cu	Fe	Ni
AZ31	Bal.	3.0	0.9	0.02	0.3	0.002	0.004	<0.002
AZ61	Bal.	5.7	0.7	0.02	0.3	<0.002	<0.002	<0.002
AZ80	Bal.	8.0	0.6	0.03	0.3	<0.002	0.002	<0.002
A6005C	0.6	Bal.	0.00	0.6	0.01	...	0.1	...

explosive welding (Ref 23, 24). The tensile pattern of residual stress at the surface is particularly undesirable, as they cause increased susceptibility to fatigue (Ref 25) and stress corrosion (Ref 26). Therefore, it is necessary to evaluate residual stresses in explosively welded multilayers. Residual stresses in engineer-

ing structures affect crack initiation, crack growth, and fracture. The exact conclusions on the state of residual stress in explosively welded multilayer structures cannot be deduced without the wide range of analyzed composite structures and the use of different methods to determine residual stresses (Ref 27, 28). In this study, the residual stress at the interface of the cladding plates with high accuracy was measured using the synchrotron radiation x-ray diffraction (XRD) method using synchrotron radiation. The $\sin^2\psi$ method was performed to estimate the in-plane residual stress.

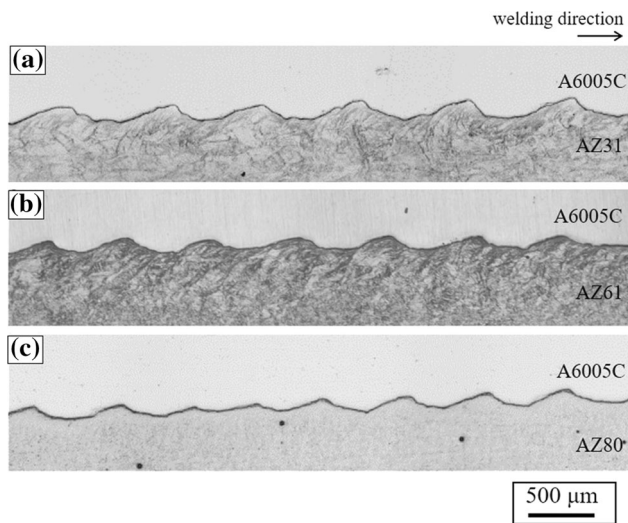


Fig. 4 Optical microscopy images for explosively welded (a) AZ31/A6005C, (b) AZ61/A6005C, and (c) AZ80/A6005C cladding plates

2. Experimental

2.1 Materials

The samples for this study were prepared from extruded materials of AZ31, AZ61, and AZ80 magnesium alloys, and A6005C aluminum alloys, with a thickness of 3 mm, a width of 130 mm, and a length of 1000 mm. Table 1 shows the chemical compositions of materials. The cladding plate was manufactured using explosive welding of magnesium alloy/aluminum alloy. Flyer and base plates were made of aluminum and magnesium alloys, respectively. As shown in Fig. 2, the base plate was located at the bottom and the explosive material was laid on the top of the flyer plate. A6005C aluminum alloy plate was placed on top of AZ31, AZ61, and AZ80 magnesium alloy plates as flyer plates. As the explosive, an ammonium nitrate

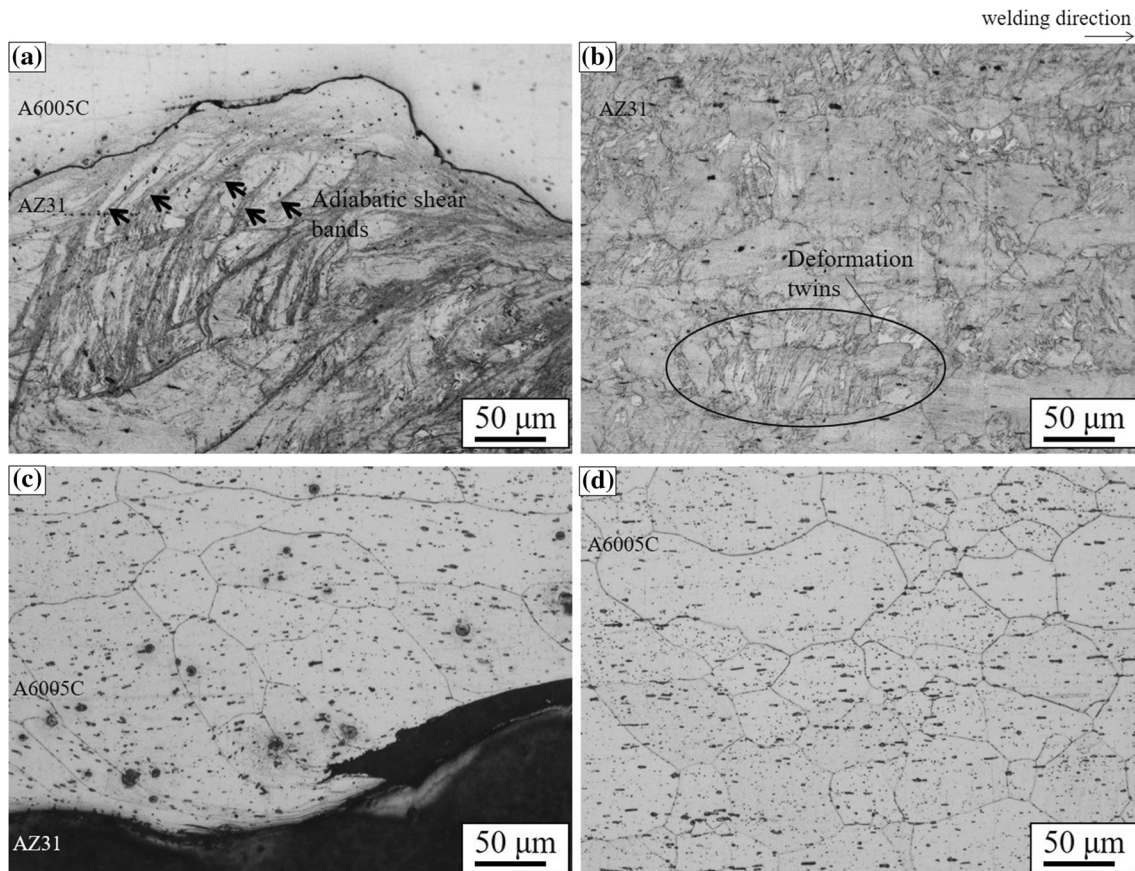


Fig. 5 Enlarged optical microscopy images for (a), (b) AZ31 and (c), (d) A6005C of the interface in explosively welded AZ31/A6005C cladding plates

oil-based explosive was used. The explosive was arranged in a sheet shape and detonated via a detonator so that the explosive impact wave propagated in a form close to a plane wave during the welding. The final thickness of the explosively welded cladding plate was ~ 5.8 mm.

2.2 Microstructural Characterizations

The explosively welded cladding plates were cut into small pieces, and the parallel cross-section in the joining direction was ground using emery papers of #800–#2000, and then polished with diamond paste and colloidal silica. The sample was etched with picric acid and the microstructure was observed using an optical microscope. In addition, using a focused ion beam processing device, small pieces are cut and picked up from the surface of the resin-embedded sample with an ion beam (40 kV, Ga⁺), fixed on a Copper mesh, and then thin-film processed to perform a transmission electron microscope (TEM) observation using JEM-2100F (JEOL). Local morphological observation of the interface of the cladding plates was performed in the scanning transmission electron microscope (STEM) mode. The Vickers hardness values were measured using an HMV-1 (Shimadzu Corporation) with a 10 g load through the bonding interface. Nanoindentation ENT-

NEXUS (ELIONIX INC.) with a low load unit was used to characterize the deformation and nanomechanical properties of the specimen. A maximum load of 1.5×10^{-3} gf with a load holding time at 1 s was used. Measured in 4 rows with 20 points in each row was selected for nanoindentation tests across the interface.

2.3 Residual Stress

Residual stress at the interface of the cladding plates was measured by the $\sin^2\psi$ method using synchrotron radiation x-rays at Aichi Synchrotron Radiation Center. Applied beamline was BL8S1 (Thin film x-ray diffraction). The stress value, σ , can be obtained by measuring the diffraction angle (2θ) while varying angle ψ . ψ is formed by sample surface normal N and lattice plane normal N' .

The optical system of the stress analyzer used in this research is the iso-inclination method. In this method, the setting plane of the ψ angle and the counter scanning (2θ scanning) plane are in the same plane. The diffraction angle is measured by aligning the ψ plane to the detector scanning (2θ scan) plane (diffraction surface). This is the method commonly used for residual stress measurement.

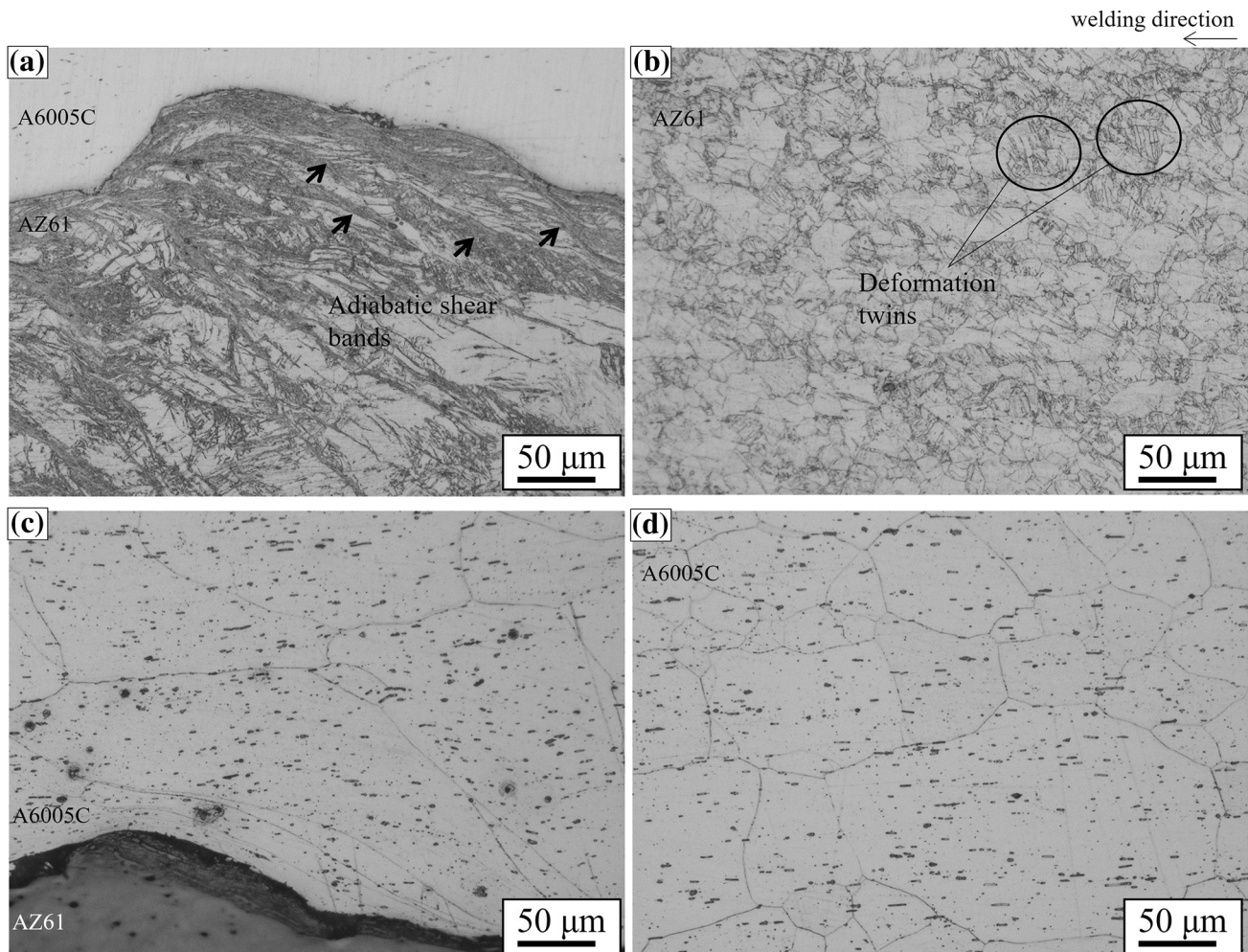


Fig. 6 Enlarged optical microscopy images for (a), (b) AZ61 and (c), (d) A6005C of the interface in explosively welded AZ61/A6005C cladding plates

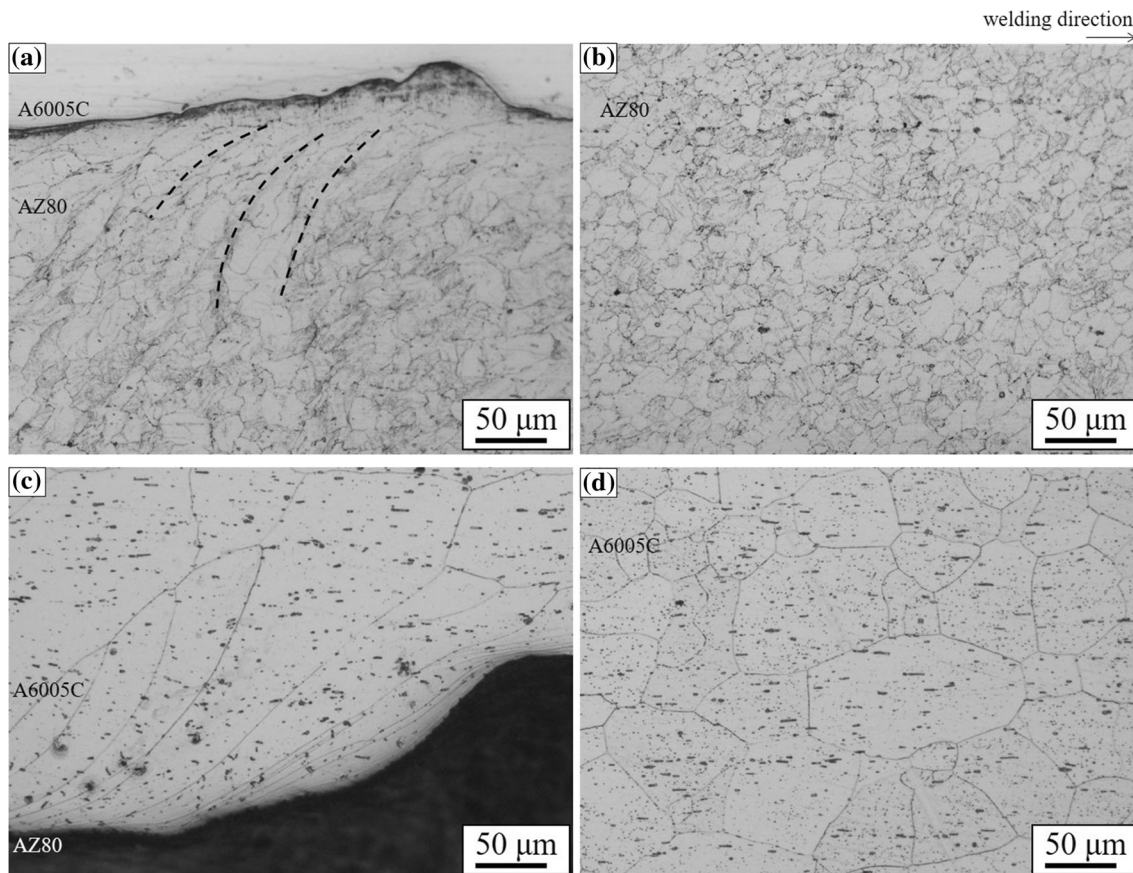


Fig. 7 Enlarged optical microscopy images for (a), (b) AZ80 and (c), (d) A6005C of the interface in explosively welded AZ80/A6005C cladding plates

The measurement surface was a cross-section parallel to the welding direction. Details of sample size, measuring direction, measuring surface, and measuring positions are shown in Fig. 3. The surface of the specimen polished with emery paper of #800 was used as the measurement surface. To select peaks for stress determination, the XRD scan was performed on the magnesium and aluminum alloys far from the interface in the range of $2\theta = 20^\circ\text{--}130^\circ$. Residual stresses estimated using the XRD method have more consistent results when performed on peaks with 2θ angles greater than 90° , multiple indices, and relatively high intensity (Ref 29). Based on these guidelines, the Al (511) and Mg (213) peaks were chosen for residual stress analysis. The measured stress direction was parallel to the welding direction. The wavelength and energy of synchrotron radiation x-ray were 0.135 nm and 9 keV, respectively.

3. Results and Discussion

3.1 Metallographic Characterization of the Interface

Figure 4 shows the cross-sectional optical images of explosively welded AZ31, AZ61, AZ80 magnesium alloys/A6005C aluminum alloy cladding plates. The interface in all samples had a wavy shape. The asymmetrical waves are attributed to the density differences in the materials used for explosive welding. The wavelength and amplitude of each sample's interface are shown in Table 2. The presented values

are the average values obtained by measuring 10 points (waves). Further, the ratios of wave amplitude to wavelength for each cladding plate are listed in Table 2. All of them are less than the well-known Karman vortex street stable spacing ratio of 0.28 (Ref 30). Ghaderi et al. investigated the effect of welding parameters such as contact point velocity, flyer plate velocity and collision angle on the morphological characteristic of the explosively welded A1100 aluminum/ AZ31 magnesium alloy joints (Ref 30). They revealed that the wavy-waveless transition occurs depending on the collision angle and collision velocity. Compared to smooth interface, wavy interface is effective for increasing shear strength of the joints due to the increment of the interfacial contact area. Ghaderi et al. also showed the existence of eddy regions or vortices close to the ascending part of the waves (Ref 30), however, in our case, they are not observed in all cladding plates. In the cladding plates using AZ31 and AZ61 (Fig. 3a and b), adiabatic shear bands are observed at the interface on the magnesium alloy side.

Figure 5 shows the cross-section optical images of the explosively welded AZ31/A6005C cladding plates. As mentioned above, adiabatic shear bands are formed at the interface on the magnesium alloy side (Fig. 5a, black arrows). It is known that magnesium has a lower thermal conductivity than aluminum, and transfer of heat induced by stress concentration is hardly occurred. Due to limited slip system originated from the hexagonal close-packed (HCP) structure, strain accumulation is tended to be occurred. For those reasons, it is considered

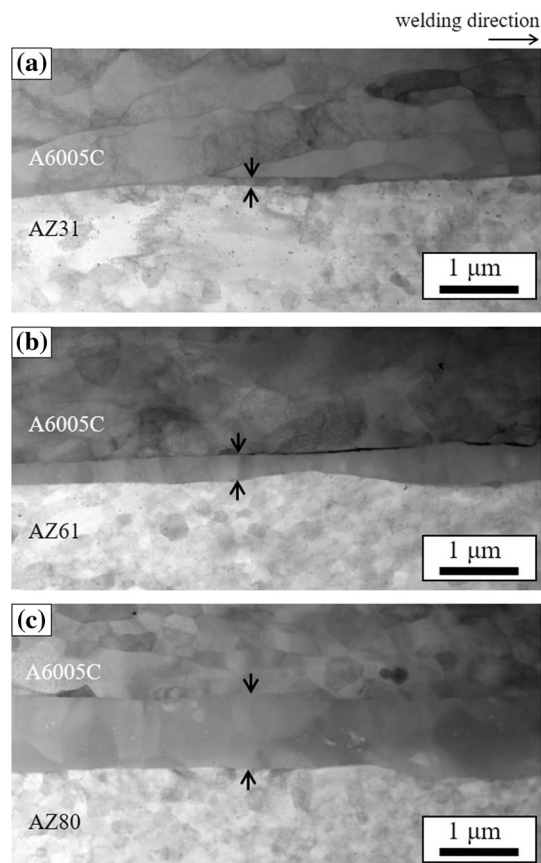


Fig. 8 Bright field STEM images of interfacial microstructure for explosively welded (a) AZ31/A6005C, (b) AZ61/A6005C, and (c) AZ80/A6005C cladding plates

that adiabatic shear bands were formed in AZ31 magnesium alloy. Deformation twins were observed over the entire cross-section in the AZ31 magnesium alloy (Fig. 5b). Formation of the deformation twins occurs due to the impact of the welding. At the interface on the aluminum side, the plastic flow of grain structure was observed (Fig. 5c). The microstructure of A6005C aluminum alloy had both coarse and fine grains (Fig. 5d).

Figure 6 shows the cross-section optical images of the explosively welded AZ61/A6005C cladding plates. Please note that in this figure the welding direction is different from Figs. 5 and 7. Similar to Fig. 5, adiabatic shear bands are formed at the interface on the magnesium alloy side (Fig. 6a, black arrows). Deformation twins were also observed over the entire cross-section (Fig. 6b), however, the grain size of magnesium alloy was much smaller than that of AZ31/A6005C cladding plates. Similar to Fig. 5(c) and (d), the plastic flow of grain structure appeared at the interface close to the aluminum side (Fig. 7c). The crystal grain structure in A6005C aluminum alloy was a mixed grain structure of coarse and fine grains (Fig. 7d). Figure 7 shows the cross-section optical images of the explosively welded AZ80/A6005C cladding plates. As shown by the broken line in Fig. 7(a), the plastic flow of the grain structure appeared on the magnesium alloy side. Deformation twins were observed only in the region up to about 500 μm below the interface (Fig. 7b). Grain size seems to be related to the

formation of deformation twins (Ref 31, 32), and the stress required for twinning increases with grain refinement according to the Hall–Petch law (Ref 33, 34). Therefore, refining ideal grain to a few microns has the effect of reducing the formation number density of deformation twins during deformation through explosive welding. It is considered that the formation of deformation twins was suppressed in AZ80 compared with AZ31 and AZ61 because the size of ideal grain was small.

3.2 Scanning Transmission Electron Microscope Observation at the Interface

Figure 8(a), (b), and (c) show the bright field STEM images of interfacial microstructure for explosively welded AZ31/A6005C, AZ61/A6005C, and AZ80/A6005C cladding plates, respectively. The interfacial layers were clearly observed for each of these materials. In AZ31/A6005C cladding plate, a thin interlayer was constantly observed at the interface, and the thickest was about 0.1 μm (Fig. 8a). Further, in the AZ61/A6005C and AZ80/A6005C cladding plates, the interlayers were formed at the interface with uniform thicknesses of 0.5 μm and 0.7 μm , respectively (Figs. 8b and c). It was found that the thickness of the intermediate layer increased with the increase in aluminum concentration at the bonding interface. However, compared to the other welding methods, the thickness of the interlayer was extremely small (Ref 4). Based on the point analysis via STEM–energy dispersive spectroscopy, compositions of the interlayer formed at the interface were close to the $\gamma\text{-Mg}_{17}\text{Al}_{12}$ phase in all the cladding plates (Fig. 9). The formation of the $\gamma\text{-Mg}_{17}\text{Al}_{12}$ phase was observed around the intermediate composition of the phase diagram shown in Fig. 1. It was reported that the $\beta\text{-Al Mg}$ and $\gamma\text{-Mg Al}$ phases was formed at a two-layer structure of the interface of laser welded magnesium alloy and aluminum alloy joints, where a heat input of laser welding is larger than that of explosive welding (Ref 35). In this study, only one-layer structure was obtained at the interface after explosive welding.

Figure 10 shows the distributions of chemical composition near the interface, which is obtained by line analysis. The interlayer is said to be a diffusion layer because of the concentration gradient. Selected area electron diffraction (SAED) patterns for the interlayer for the explosively welded AZ31/A6005C, AZ61/A6005C, and AZ80/A6005C cladding plates show halo patterns in addition to the spots of lattice reflection (Fig. 11). Point analysis and diffraction patterns suggest the formation of intermetallic compounds and the mixture of crystalline and amorphous phases, and it is considered that those are mixed to form the interlayer at the interface of cladding plates. Since the obtained SAED patterns are quite similar to the patterns of $\beta\text{-Al}_3\text{Mg}_2$ and $\gamma\text{-Mg}_{17}\text{Al}_{12}$ phases, it was impossible to identify the phase based on SAED patterns.

3.3 Hardness and Nanomechanical Properties of the Explosively Welded Cladding Plates

Figure 12 shows the hardness profiles of the interface for the explosively welded AZ31/A6005C and AZ80/A6005C cladding plates. In both cladding plates, the aluminum alloy showed higher hardness than the magnesium alloys, and the hardness increased as it approached the interface. Yan et al. reported that the remarkable decrease in the hardness due to over aging of

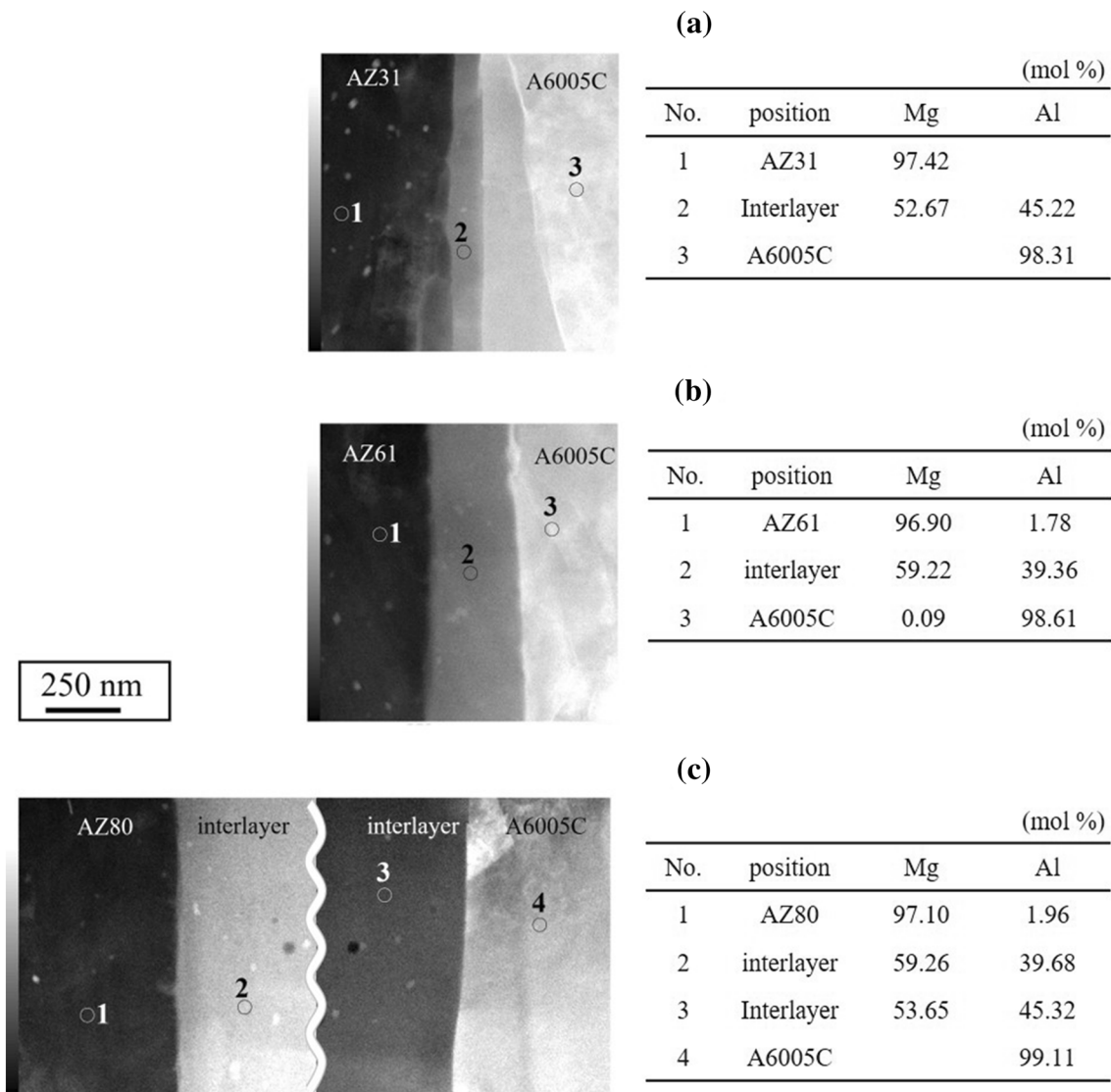


Fig. 9 Positions and results of point analysis for explosively welded (a) AZ31/A6005C, (b) AZ61/A6005C, and (c) AZ80/A6005C cladding plates

7075 aluminum alloy near the interface was observed in the explosively welded 7075/AZ31 cladding plate (Ref 36). In our case, no such decrease in hardness was seen in A6005C. In Fig. 12, the hardness of each of the AZ31, AZ80, and A6005C extruded materials is shown by the dashed line for reference. The hardness of as-extruded AZ80 magnesium alloy was higher than that of as-extruded AZ31 magnesium alloy. After explosive welding, the hardness of magnesium alloys increased in each cladding plate. In the magnesium alloys, the increase of hardness near the interface is considered to be due to the interaction of a softening caused by the adiabatic temperature rise and a strain-hardening caused by the plastic deformation during explosive welding (Ref 37). On the other hand, both shear band and twin formation in the magnesium alloy can contribute to the plastic deformation hardening. The accumulation of stress due to the difference in the coefficient of thermal expansion between magnesium and aluminum also can contribute to the hardening (Ref 38). While adiabatic shear bands were not clearly observed in Fig. 7, deformation twins were observed in the relatively small area

compared to Fig. 5 and 6. Thus, it can be assumed that the strain-hardening was likely occurred in our case. After explosive welding, the hardness of aluminum alloy also increased in each cladding plate, although the hardness in each cladding plate showed a different tendency. The hardness of A6005C aluminum alloy in AZ80/A6005C cladding plate was larger than that of A6005C aluminum alloy in AZ31/A6005C cladding plate at all measurement points. Due to the difference in tensile properties of magnesium alloys (AZ31 and AZ80 magnesium alloys), the degree of strain-hardening might be changed resulting in the different hardness of A6005C aluminum alloy after explosive welding. Also, since A6005C aluminum alloy is an age-hardenable alloy, the precipitation hardening state may be different in each cladding plate.

In order to investigate the nanomechanical properties of the interface of explosively welded cladding plate, nanoindentation tests were performed for the explosively welded AZ80/A6005C cladding plate. Figure 13 shows the profiles of the nano-hardness across the interface for the explosively welded AZ80/A6005C cladding plates. Each symbol represents each

measurement line. On the A6005C aluminum alloy side, the variation of hardness was large. No increase in hardness was confirmed at the interface, which was different tendency with Fig. 12. The hardness values obtained at the interface were almost the same as that of the AZ80 magnesium side. The Vickers hardness is considered to be affected by the internal stress caused by the change in the microstructure and the plastic deformation caused by the slip line. Further, the hardness obtained by using the nanoindentation test can be influenced by the micro nano behavior of the interface, and the non-uniform hardness distribution in A6005C aluminum may confirm the nonuniformity of the interface morphology. The hardness of AZ80 magnesium alloy,

A6005C aluminum alloy, and the interface was 0.87, 3.48, and 1.21 GPa, respectively. There was no significant difference in hardness and deformation behavior between the AZ80 magnesium and the interface. Thus, it was found that the γ -Mg₁₇Al₁₂ phase formed at the interface was likely not a significantly brittle structure as compared with the AZ80

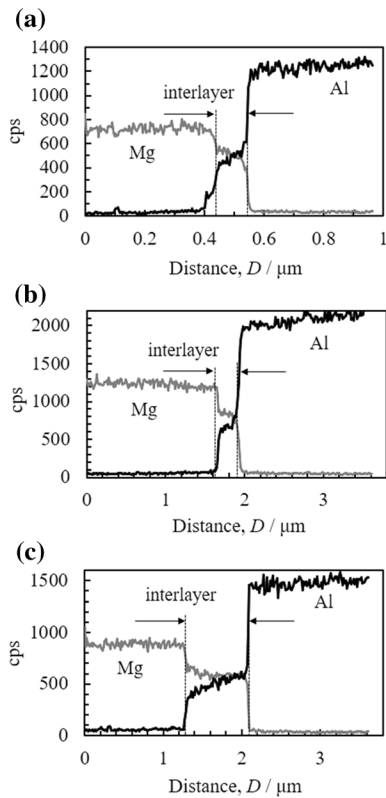


Fig. 10 Distributions of chemical composition near the interface obtained by line analysis for explosively welded (a) AZ31/A6005C, (b) AZ61/A6005C, and (c) AZ80/A6005C cladding plates (Ref 22)

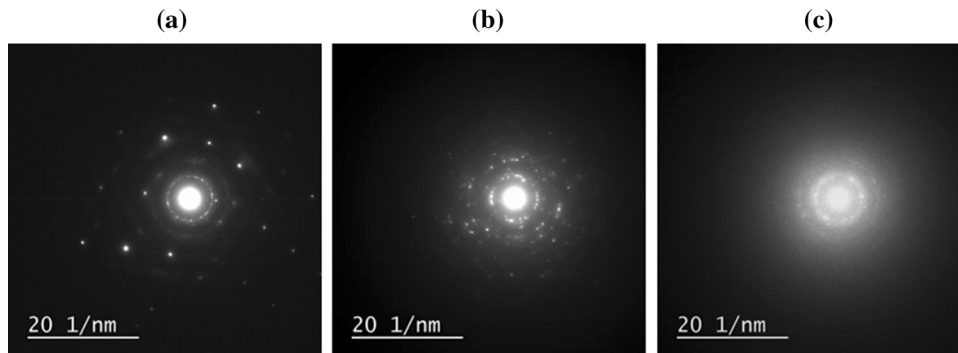


Fig. 11 Selected area electron diffraction (SAED) patterns for the interlayer for the explosively welded (a) AZ31/A6005C, (b) AZ61/A6005C and (c) AZ80/A6005C cladding plates (Ref 22)

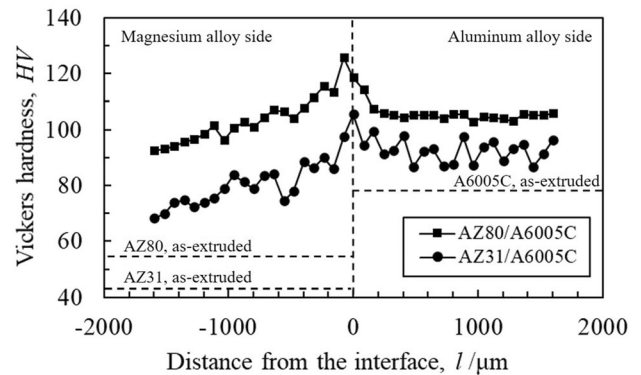


Fig. 12 Profiles of the Vickers hardness across the interface for the explosively welded AZ31/A6005C and AZ80/A6005C cladding plates

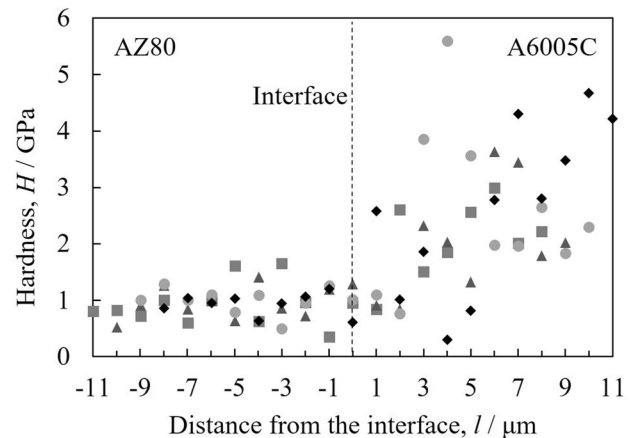


Fig. 13 Profiles of the nano hardness across the interface for the explosively welded AZ80/A6005C cladding plates. Each symbol represents each measurement line

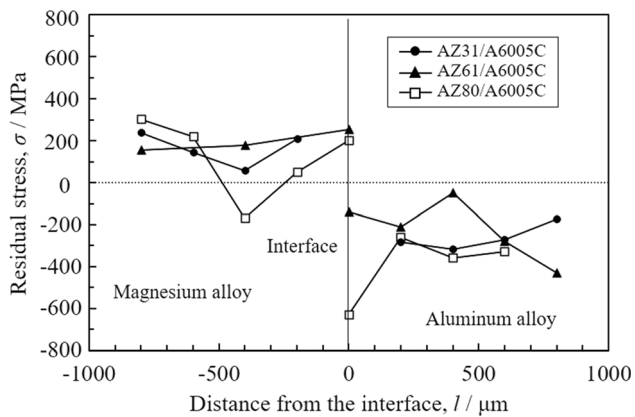


Fig. 14 Profiles of the residual stress across the interface of the explosively welded AZ31/A6005C, AZ61/A6005C, and AZ80/A6005C cladding plates

magnesium alloy and A6005C aluminum alloy matrix.

3.4 Distributions of Residual Stress at the Interface

Residual stress measurements were performed using synchrotron radiation x-rays. Figure 14 shows the obtained residual stress values calculated from the slope of the linear fit of the $\sin^2\psi$ plots. In all cladding plates, the residual stress on the magnesium alloy side and the aluminum alloy side were the tensile stress and the compressive stress, respectively.

It has been reported that in the case of dissimilar materials, residual stresses are further enhanced by differences in elastic properties and CTE among the base and flyer materials (Ref 39). As reported in the previous study, in the case of the distribution of residual stress in the Al/Cu/Al multilayers manufactured by explosive welding, the surface (aluminum layer) is subjected to a high tensile residual stress state (Ref 40). The elastic elongation of the aluminum layer is higher than the copper layer due to their different elasticity modules, which has affected the evolution of tensile residual stress at the surface (aluminum layer). However, the residual stresses associated with the welding of dissimilar materials with similar stiffness are often connected to differences in CTE among the base materials. In our case, compressive residual stress was obtained at the surface (A6005C aluminum alloy) of explosively welded cladding plates. It can be attributed to the difference in the CTE of magnesium and aluminum. It is considered that the material with a small CTE (aluminum alloy) restrained the contraction of the material with a large CTE (magnesium alloys) in the high-speed deformation at the time of the explosion, and then the residual stress was generated. For further discussion, it is necessary to clarify the origin of the residual stress distribution by measuring the explosive welded material made from the materials having a similar CTE. Accordingly, the cutting method, location of the measuring points, detonation velocity affect the residual stress distribution (Ref 24, 27, 41). For the detailed analysis of the residual stress formation process, evaluation by combining three-dimensional analysis by the neutron diffraction method and prediction by the finite element method is required.

4. Conclusive Summary

The effect of magnesium alloy composition on the evolution of interfacial microstructure, hardness, and nanomechanical properties of explosively welded magnesium alloy/aluminum alloy cladding plates was investigated. The following points can be highlighted:

1. A wavy interface was observed in all the explosively welded cladding plates. The interlayer composed of the $\gamma\text{-Mg}_{17}\text{Al}_{12}$ phase was formed at the interface. The higher aluminum concentration in the magnesium alloy leads to the thicker intermediate layer.
2. In the cross-section of the cladding plate, aluminum alloy showed a relatively high hardness compared with the magnesium alloy, and the hardness values increased as it approached the interface.
3. Through nanoindentation tests, no increase in hardness was confirmed at the interface. Hardness at the interface is almost the same as that on the magnesium alloy side. The Vickers hardness is considered to be affected by the internal stress caused by the change in the microstructure and the plastic deformation caused by the slip line. Further, the hardness obtained using the nanoindentation test is influenced by the micro-nano behavior of the interface.
4. The residual stress on the magnesium alloy side and the aluminum alloy side were the tensile stress and the compressive stress, respectively. It is considered that the material with a small linear expansion coefficient (aluminum alloy) restrained the contraction of the material with a large linear expansion coefficient (magnesium alloys) in the high-speed deformation at the time of the explosion.

Acknowledgments

We would like to express our gratitude for the support of the Grant-in-Aid for Scientific Research (Young Researcher: No. 21K14425), Light Metal Scholarship Society, and Aluminum Association. The residual stress in this study was measured at BL8S1 of the Aichi Science and Technology Foundation Aichi Synchrotron Optical Center (Experiment No.: 202102068), and the TEM observation was performed at the Aichi Industrial Science and Technology Center.

Open Access

This article is licensed under a Creative Commons Attribution 4.0 International License, which permits use, sharing, adaptation, distribution and reproduction in any medium or format, as long as you give appropriate credit to the original author(s) and the source, provide a link to the Creative Commons licence, and indicate if changes were made. The images or other third party material in this article are included in the article's Creative Commons licence, unless indicated otherwise in a credit line to the material. If material is not included in the article's Creative Commons licence and your intended use is not permitted by statutory regulation or exceeds the permitted use, you will need to obtain permission directly from the copyright holder. To view a copy of this licence, visit <http://creativecommons.org/licenses/by/4.0/>.

References

- F. Liu, D. Ren and L. Liu, Effect of Al foils interlayer on microstructures and mechanical properties of Mg-Al butt joints welded by gas tungsten arc welding filling with Zn filler metal, *Mater. Des.*, 2013, **46**, p 419–425
- M.J. Fernandes, T. Senthilkumar, V. Balasubramanian and S. Rajakumar, Optimizing Diffusion Bonding Parameters to Maximize the Strength of AA6061 Aluminum and AZ31B Magnesium Alloy Joints, *Mater. Des.*, 2012, **33**, p 31–41
- B. Zhu, W. Liang and X.R. Li, Interfacial Microstructure, Bonding Strength and Fracture of Magnesium-Aluminum Laminated Composite Plates Fabricated by Direct Hot Pressing, *Mater. Sci. Eng. A*, 2011, **528** (21), p 6584–6588
- N. Yamamoto, J. Liao, S. Watanabe and K. Nakata, Effect of Intermetallic Compound Layer on Tensile Strength of Dissimilar Friction Stir Weld of a High Strength Mg Alloy and Al Alloy, *Mater. Trans.*, 2009, **50**(12), p 2833–2838
- T. Morishige, A. Kawaguchi, M. Tsujikawa, M. Hino, T. Hirata and K. Higashi, Dissimilar Welding of Al and Mg Alloys by FSW, *Mater. Trans.*, 2008, **49**(5), p 1129–1131
- B.M. Thaddeus, Binary Alloy Phase Diagrams, 2nd ed., B.M. Thaddeus, Ed., ASM International, 1990, p 169–171
- T. Onzawa, 爆発圧接結合界面における波形成の機構について (The Mechanism of Wave Formation in Explosively Bonded Interface), *J. Japan High Press. Inst.*, 1975, **13**(2), p 103–109. (in Japanese)
- V.I. Lysak and S.V. Kuzmin, Energy Balance During Explosive Welding, *J. Mater. Process. Tech.*, 2015, **222**, p 356–364
- T.Z. Blazynski, Explosive Welding, Forming and Compaction, Elsevier, New York, 1983
- I.A. Bataev, S. Tanaka, Q. Zhou, D.V. Lazurenko, A.J. Junior, A.A. Bataev and P. Chen, Towards Better Understanding of Explosive Welding by Combination of Numerical Simulation and Experimental Study, *Mater. Des.*, 2019, **169**, p 107649
- M. Otsuka, 爆発圧着クラッドを用いた異材継手 (Transition Joints Using Explosive Welding Clad), *Journal of Japan High Pressure Institute*, 2015, **53**(1), p 42–45. (in Japanese)
- Y. Ming, J. Xu, H. Ma, M. Lei, X. Ni, Z. Shen, B. Zhang and J. Tian, Microstructure Development During Explosive Welding of Metal Foil: Morphologies Mechanical Behaviors and Mechanisms, *Compos. Part B*, 2021, **212**, p 108685
- Y. Ming, H. Ma, Z. Shen, Z. Huang, Q. Tian and J. Tian, Dissimilar Material Welding of Tantalum Foil and Q235 Steel Plate Using Improved Explosive Welding Technique, *Mater. Des.*, 2020, **186**, p 108348
- Y. Ming, J. Xu, D. Chen, H. Ma, Z. Shen, B. Zhang and J. Tian, Understanding Interface Evolution During Explosive Welding of Silver Foil and Q235 Substrate Through Experimental Observation Coupled with Simulation, *Appl. Surf. Sci.*, 2021, **566**, p 150703
- H. Paul, J. Morgiel, T. Baudin, F. Brisset, M. Prazmowski and M. Miszczyk, Characterization of explosive weld joints by TEM and SEM/EBSD, *Arch. Metall. Mater.*, 2014, **59**(3), p 1129–1136
- H. Zhang, K.X. Jiao, J.L. Zhang and J.P. Liu, Comparisons of the microstructures and micro-mechanical properties of copper/steel explosive-bonded wave interfaces, *Mater. Sci. Eng. A*, 2019, **756**, p 430–441
- M. Yang, H. Ma, Z.W. Shen, D.G. Cheng and Y.X. Deng, Microstructure and mechanical properties of Al-Fe meshing bonding interfaces manufactured by explosive welding, *T. Nonferr. Metal. Soc.*, 2019, **29**(4), p 680–691
- G.H.S.F.L. Carvalho, I. Galvo, R. Mendes, R.M. Leal and A. Loureiro, Explosive Welding of Aluminium to Stainless Steel Using Carbon Steel and Niobium Interlayers, *J. Mater. Process Technol.*, 2020, **283**, p 116707
- H. Zhang, K.X. Jiao, J.L. Zhang and J.P. Liu, Microstructure and mechanical properties investigations of copper-steel composite fabricated by explosive welding, *Mater. Sci. Eng. A*, 2018, **731**, p 278–287
- T. Zhang, W. Wang, W. Zhang, J. Zhou and Z. Yan, Interfacial Microstructure Evolution and Deformation Mechanism in an Explosively Welded Al/Mg Alloy Plate, *J. Mater. Sci.*, 2019, **54**, p 9155–9167
- M. Sahul, M. Sahul, J. Lokaj, L. Caplovic, P. Nesvadba and B. Odokienova, The Effect of Annealing on the Properties of AW5754 Aluminum Alloy-AZ31B Magnesium Alloy Explosively Welded Bimetals, *J. Mater. Eng. Perform.*, 2019, **28**, p 6192–6208
- K. Asai, M. Narita, H. Sato, Y. Watanabe, H. Mori, N. Saito, I. Nakatsugawa and Y. Chino, マグネシウム/アルミニウム合金爆発圧着材の界面組織、耐食性および機械的性質に及ぼす マグネシウム合金組成の影響 (Effect of magnesium alloy compositions on the interfacial microstructure, corrosion resistance and mechanical properties of explosively welded magnesium/aluminum alloys), *J. Jpn. Inst. Light Met.*, 2022, **72**(5). (in Japanese)
- A. Karolczuk, M. Kowalski, K. Kluger and F. Zok, Identification of Residual Stress Phenomena Based on the Hole Drilling Method in Explosively Welded Steel-Titanium Composite, *Arch. Metall. Mater.*, 2014, **59**(3), p 1119–1123
- N. Li, M. Zhang, J. Ye, C. Liu and C. Liu, Experimental Investigation on Residual Stress Distribution in Zirconium/Titanium/Steel Tri-Metal Explosively Welded Composite Plate After Cutting and Welding of a Cover Plate, *J. Manuf. Processes*, 2021, **64**(2), p 455–463
- M.N. James, D.J. Hughes, Z. Chen, H. Lombard, D.G. Hattingh, D. Asquith, J.R. Yates and P.J. Webster, Residual Stress and Fatigue Performance, *Eng. Fail. Anal.*, 2007, **14**(2), p 384–395
- M. Mochizuki, Control of Welding Residual Stress for Ensuring Integrity Against Fatigue and Stress-Corrosion Cracking, *Nucl. Eng. Des.*, 2007, **237**(2), p 107–123
- A. Karolczuk, H. Paul, Z. Szulc, K. Kluger, M. Najwer and G. Kwiatkowski, Residual Stresses in Explosively Welded Plates Made of Titanium Grade 12 and Steel With Interlayer, *J. Mater. Eng. Perform.*, 2018, **27**, p 4571–4581
- A. Karolczuk, K. Kluger, S. Derda, M. Prazmowski and H. Paul, Influence of Impact Velocity on the Residual Stress, Tensile Strength, and Structural Properties of an Explosively Welded Composite Plate, *Materials*, 2020, **13**(12), p 2686
- Q. Luo and S. Yang, Uncertainty of the x-ray Diffraction (XRD) $\sin^2 \psi$ Technique in Measuring Residual Stresses of Physical Vapor Deposition (PVD) Hard Coatings, *Coatings*, 2017, **7**(8), p 128
- S.H. Ghaderi, A. Mori and K. Hokamoto, Analysis of Explosively Welded Aluminum-AZ31 Magnesium Alloy Joints, *Mater. Trans.*, 2008, **49**(5), p 1142–1147
- I.J. Beyerlein, L. Capolungo, P.E. Marshall, R.J. McCabe and C.N. Tome, Statistical Analyses of Deformation Twinning in Magnesium, *Philos. Mag.*, 2010, **90**(16), p 2161–2190
- J. Wang, I.J. Beyerlein and C.N. Tome, An Atomic and Probabilistic Perspective on Twin Nucleation in Mg, *Scr. Mater.*, 2010, **63**(7), p 741–746
- D. Hull, Effect of Grain Size and Temperature on Slip, Twinning and Fracture in 3% Silicon Iron, *Acta Metall.*, 1961, **9**(3), p 191–204
- M.J. Marcinkoski and H.A. Lipsitt, The Plastic Deformation of Chromium at Low Temperatures, *Acta Mater.*, 1962, **10**(2), p 95–111
- K. Matsumoto, A. Nishimoto, T. Ishikawa, K. Nagatsuta, K. Ito, M. Tsukamoto and K. Nakata, Dissimilar Materials Joining of A6061 Al Alloy and AZ31 Mg Alloy by Laser Welding, *J. Light Metal Welding*, 2019, **57**, p 198–206
- Y.B. Yan, Z.W. Zhang, W. Shen, J.H. Wang, L.K. Zhang and B.A. Chin, Microstructure and Properties of Magnesium AZ31B-Aluminum 7075 Explosively Welded Composite Plate, *Mater. Sci. Eng. A*, 2010, **527**, p 2241–2245
- Y. Yang, Z. Xinming, L. Zhenghua and L. Qingyun, Adiabatic Shear Band on the Titanium Side in the Ti/Mild Steel Explosive Cladding Interface, *Acta Mater.*, 1996, **44**(2), p 561–565
- M. Paramsothy, N. Srikanth and M. Gupta, Solidification Processed Mg/Al Bimetal Macrocomposite: Microstructure and Mechanical Properties, *J. Alloys Compd.*, 2008, **461**(1–2), p 200–208
- R. Varavallo, V.M. Moreira, V. Paes, P. Brito, J. Olivares and H.C. Pinto, Welding Induced Residual Stresses in Explosion Cladded AL-6XN Superaustenitic Stainless Steel and ASME SA516-70 Steel Composite Plates, *Adv. Mater. Res.*, 2014, **996**, p 451–456
- M. Sedighi and M. Honaripisheh, Experimental Study of Through-Depth Residual Stress in Explosive Welded Al-Cu-Al Multilayer, *Mater. Des.*, 2012, **37**, p 577–581
- A. Karolczuk, M. Kowalski, K. Kluger and F. Zok, Identification of residual stress phenomena based on the hole drilling method in explosively welded steel-titanium composite, *Arch. Metall. Mater.*, 2014, **59**(3), p 1129–1133

Publisher's Note Springer Nature remains neutral with regard to jurisdictional claims in published maps and institutional affiliations.